Real-time monitoring of cell adhesion on to a soft substrate by a graphene impedance biosensor

Victoria Guglielmotti[1,2§], Emil Fuhry[1§], Tilmann J. Neubert[1], Michel Kuhl[1], Diego Pallarola[2*], Kannan Balasubramanian[1*]

[1]Department of Chemistry, School of Analytical Sciences Adlershof (SALSA) & IRIS Adlershof, Humboldt-Universität zu Berlin, Berlin, Germany.

[2]Instituto de Nanosistemas, Universidad Nacional de General San Martín, San Martín, 1650 Provincia de Buenos Aires, Argentina

[§] Equal Contribution

Corresponding author e-mail: dpallarola@unsam.edu.ar , nano.anchem@hu-berlin.de

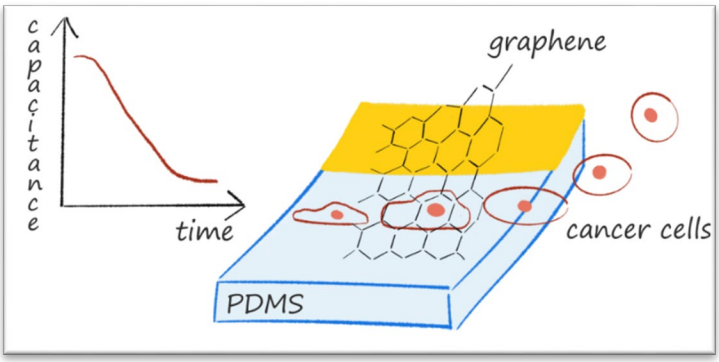

ABSTRACT

Soft substrates are interesting for a range of applications from mimicking cellular micro-environment to implants. Conductive electrodes on soft substrates open a broad spectrum of possibilities such as electrical and electrochemical sensing coupled with the flexibility, elasticity and transparency of the underlying substrate. Single layer graphene on a soft substrate as a candidate for such flexible electrodes brings the additional advantage that the active area of the sensor is transparent and conformal to the underlying substrate. Here, we overcome several challenges facing the routine realization of graphene cell sensors on a canonical soft

substrate namely poly(dimethylsiloxane) (PDMS). Specifically, we have systematically studied the effect of surface energy before, during and after the transfer of graphene. Based on this, we have identified a suitable support polymer, optimal substrate (pre-) treatment and an appropriate solvent for the removal of the support. Using this procedure, we can reproducibly obtain stable and intact graphene sensors in millimeter-scale on PDMS, which can withstand continuous measurements in cell culture media for several days. From local nanomechanical measurements with an AFM, we infer that the softness of the substrate is slightly affected after graphene transfer. However, we can modulate the stiffness using PDMS of differing composition. Finally, we show that graphene sensors on PDMS can be successfully used as electrodes for real-time monitoring of cell adhesion kinetics on a soft substrate. The routine availability of single layer graphene electrodes on a flexible soft substrate with tunable stiffness will open a new avenue for a range of studies, where the PDMS-liquid interface is made conducting with minimal alteration of the intrinsic material properties such as softness, flexibility, elasticity and transparency.

INTRODUCTION

Soft substrates provide many advantages for bioanalysis such as the possibility to mimic tissues, emulating the cellular microenvironment [1] and as flexible and soft biosensors. [2-6] Several efforts are underway to integrate (bio)electronic devices on synthetic soft materials, among which PDMS is a widely used candidate. [7-8] One important advantage of using PDMS is that the Young's modulus can be varied over nearly an order of magnitude by just varying the composition, characterized by the base to curing agent ratio (BCA-ratio) and the curing temperature. [9-11] In this manner, the cellular response can be systematically studied by modulating the stiffness of the extracellular environment.

There are several successful demonstrations of bioelectronic devices on PDMS, [7] often utilizing standard metal deposition techniques using gold or other metals. The effect of using such

materials on the ensuing stiffness of PDMS must not be overlooked. In many cases, the goal is to obtain flexibility, for which the change in stiffness brought about by the deposited material is not that relevant. On the other hand, if we are interested in applications where we would like to provide a cellular microenvironment with a desired stiffness, it is crucial to characterize the effect of the electrode material on the stiffness. It has been shown that even thin metallic layers on PDMS increase the stiffness by more than four orders of magnitude. [12] Hence, there is a need for electrodes made from alternative materials, which do not modify the favorable stiffness properties of PDMS significantly.

On the other hand, it is well established that cellular behavior and interactions are affected by the stiffness of the underlying substrate to a considerable extent. [2, 13-15] Also, for the study of such interactions, it is particularly important that the substrate stiffness does not deviate drastically upon inclusion of a sensing electrode. Soft electrodes have been realized on PDMS using organic conducting polymers such as PEDOT (poly(3,4-ethylenedioxythiophene)). [16] However, they are several nanometers thick and are often non-transparent and hence do not allow for concurrent optical imaging of cell behavior in transmission mode. While such materials are known to exhibit high elastic modulus, [17] the changes in mechanical properties of PDMS due to such materials have seldom been systematically investigated.

Monolayer graphene as an electrode is an ideal candidate to be evaluated for realizing soft bioelectronic devices on PDMS. [18] Among several conducting materials, graphene provides the key advantage that a very good conducting layer is achieved with just a single layer of carbon atoms. Coupled with the pure carbon-based framework, it can be expected that such a layer could provide the smallest change in stiffness because of an electrode. In addition, the flexibility and transparency of the underlying PDMS is totally guaranteed. [19] For obtaining graphene-based soft bioelectronic devices, it is necessary to obtain graphene on PDMS substrates (of varying stiffness) at a large scale, without breaks or cracks and with minimal contamination. Chemical vapor deposited (CVD) graphene is the source material of choice, since it can be

procured in large amounts and several transfer methods exist, to obtain CVD-graphene sheets on arbitrary substrates. [20-24] However, obtaining large-area graphene with intact regions in the mm- or cm-scale on PDMS for use as long-term routine sensors in a liquid environment or in cell culture media still faces some challenges, as discussed below.

CVD-graphene is grown typically on a catalytically active metal film or sheet (typically copper). The transfer to a chosen substrate involves mainly two steps – delamination from the copper surface using a suitable polymer support and relamination to a target surface with removal of the polymer support. [25-26] For obtaining graphene on PDMS (Gr/PDMS), two strategies are worth exploring. In the first case, PDMS can be directly used to delaminate graphene from the copper surface. On the other hand, we could use another polymer to delaminate graphene, followed by relamination on to PDMS. Since the early phase of graphene research, PDMS has been used to delaminate graphene from copper. [27-30] Optionally, an intermediate layer between graphene and PDMS is used to improve or weaken adhesion. [31-33] The change in the stiffness of PDMS brought about by these layers has seldom been systematically investigated. With dried PDMS, pressure has to be applied when attaching a PDMS sheet on to Gr/Cu, which inevitably results in a high density of cracks or breaks in the transferred graphene sheet. [20] To avoid this problem, it was proposed that the base/curing agent mixture could be first poured on to the Gr/Cu sheet and subsequently cured. [34] The main issue with the direct delamination approach is that the hardened PDMS displays lower adhesion to graphene. In fact, this physical aspect has been exploited to release graphene from PDMS in a facile manner on to other hard substrates such as SiO_2 or glass. [25] This low adhesion to PDMS is indeed a problem for graphene sensors operating in liquid, since the attached graphene sheet is not stable in buffers, cell culture media or extreme acidic / basic conditions. Moreover, it is difficult to tune the stiffness of underlying PDMS using this approach.

The second strategy involving the use of a different polymer to delaminate and subsequently relaminate on to PDMS appears to be more suitable. In this context, there are two fundamental

issues. The relamination is typically carried out in water. First, the low surface energy of PDMS limits wetting of the surface by water, which prohibits an intimate contact between graphene and as-prepared PDMS in the aqueous environment. [18, 31, 35] Moreover, the interaction energy between graphene and PDMS is too low to promote good and persistent adhesion. On rigid substrates such as silicon oxide, an annealing treatment at high temperatures ensures a persistently good adhesion, while at the same time ensuring a clean graphene surface. [36-38] On PDMS, however, we are limited by a temperature of 120°C, beyond which morphological changes occur, deforming the substrate irreversibly. [39] Secondly, PDMS is generally very sensitive to several organic solvents. [18, 40] For the removal of the support polymer, the PDMS substrate is typically exposed to acetone or toluene, which causes a swelling of the substrate. [41] Since the adhesion between graphene and the PDMS (as-prepared) is very low, the swelling inevitably leads to a detachment of most areas of the graphene sheet. In some cases, even dipping the Gr/PDMS assembly in water leads to a destruction of the graphene sheet because of the low adhesion. In principle, we need to optimize the surface energy or interfacial interactions at every stage during the relamination process. [25, 33] Here, we have taken a systematic approach to attack this problem and show that by optimizing the interaction energy between graphene and PDMS, it is indeed possible to realize stable graphene sensors on PDMS of varying stiffness.

As a proof-of-principle, we have chosen to deploy the realized graphene sensors to detect the real-time kinetics of cell adhesion on to the soft PDMS substrate. It has been proposed that the the adhesion kinetics of cells on to substrates depend often on the stiffness of the underlying substrate. Typically, one can use optical or fluorescence microscopy to study the growth of cells on a given substrate. [42-44] Alternatively, methods such as electrochemical impedance spectroscopy (EIS), [45] electrical cell-substrate impedance spectroscopy (ECIS) [46-48] or quartz crystal microbalance [49] (QCM) can be used, which offer the major advantage that we can observe the evolution of adhesion in real time with an improved time resolution. The realized

graphene electrodes on PDMS are ideally suited as electrodes in EIS, using which we can monitor the interactions of cells with the soft elastic Gr/PDMS surface. We show that using such a setup, the different phases of cell adhesion can be deciphered from the real-time impedance spectra.

RESULTS and DISCUSSION

First, we discuss the results obtained for the transfer of graphene on to PDMS prepared with a base to curing agent ratio (BCA-ratio) of 10:1 (w/w) and using a standard polymer-assisted wet transfer method. [50] Shortly, graphene on a copper substrate was coated with a desired support polymer (e.g. polystyrene). Subsequently copper is etched away in an acidified peroxide solution. The polymer/graphene stack is then transferred to a desired substrate and the upper polymer layer removed in an appropriate solvent (toluene for removing polystyrene). More details can be found in the Methods section. The use of this procedure without any pre- or post-treatment of the PDMS substrate resulted usually in a graphene layer that was not intact. Only very small areas of the original graphene sheet were attached to the PDMS surface, while the rest rolled up or completely detached during the transfer process (see optical image in figure S1 in supporting information (SI)).

Several strategies have been reported to modulate the surface energy of PDMS. [51-53] We focused here on the use of oxygen plasma, [54-55] which predominantly introduces silanol groups rendering the surface polar. On the other hand, the wetting of the PDMS surface can then be monitored by contact angle measurements. [56] Contact angles measured on a PDMS sample after plasma treatment by varying the plasma power and duration are shown in figures 1(a) and 1(b) respectively. The contact angle of water on as-prepared PDMS (corresponding to duration = 0 s and power = 0 W) is more than 90° signifying a low surface energy and poor wettability. As the duration and intensity of the plasma treatment increases, we clearly see a reduction in the measured contact angle, consistent with a decrease in surface energy. Graphene transfer was

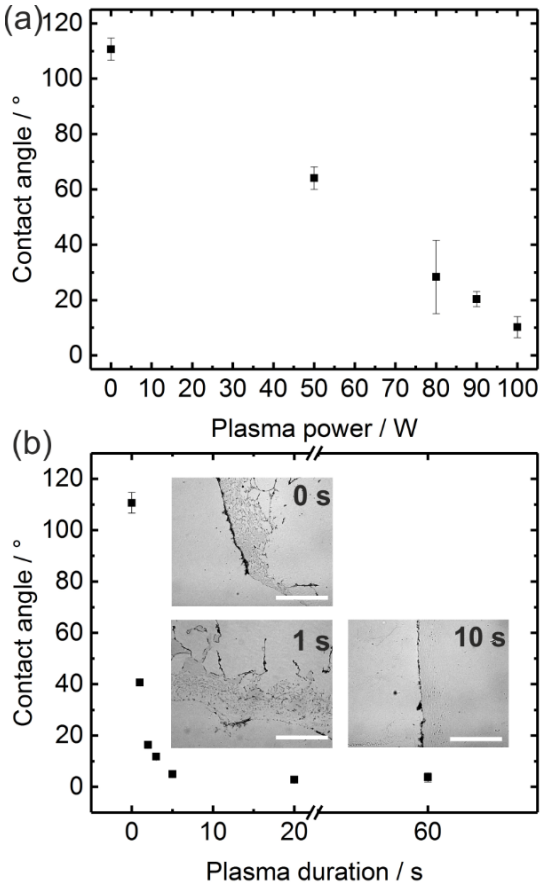

Figure 1. (a,b) Water contact angle measured on PDMS (BCA-ratio 10:1) as a function of the parameters of oxygen plasma treatment: (a) plasma power used for a constant duration of 1 s and (b) duration of plasma treatment at a constant power of 50 W. For all cases, the O_2 pressure was 0.3 mbar. The insets in (b) show optical images of graphene sheets transferred on to PDMS after using oxygen plasma treatment for the indicated conditions. Scale bar is 50 µm.

carried out on such PDMS samples after plasma treatment and the quality of transferred graphene was evaluated by optical microscopy. Optical images on selected samples are shown in the inset of figure 1(b). It is apparent that, on as-prepared PDMS as well as on PDMS exposed to a short (< 4 s) plasma treatment, graphene is not contiguous and is prone to breaks. Intact graphene sheets could be obtained after 4s of exposure to O_2 plasma. This duration corresponds to the point where the contact angle reaches a plateau due to the plasma treatment (figure 1(b)). We found that there is also an upper limit for the duration and the intensity of plasma, which can be used without causing damage to the PDMS substrate. Long time plasma exposure and high plasma intensity induce irreversible changes in surface morphology, as inferred from optical images (see figure S2 in SI). Moreover, we observed that, after such a prolonged

treatment, the polymer gets brittle and the swelling of PDMS becomes more prominent in organic solvents. Best results were obtained for a plasma duration of 6 s, a power of 40 W and a chamber pressure of 0.03 mbar. Moreover, it was necessary to carry out graphene transfer immediately after the plasma treatment.

The final step in graphene transfer involves the removal of the support polymer (e.g. polystyrene in figure 1). This has to be carried out in an organic solvent (toluene) to ensure a clean graphene surface. Moreover, the swelling has to be kept to a minimum, so that the transferred monolayer is neither damaged nor detached. Several support polymer/solvent combinations were studied. The suitability of the combination was evaluated by obtaining optical images after the graphene transfer (see figure S3 in SI). We found that polystyrene as polymer support and ethyl acetate as the remover satisfied the afore-mentioned requirements to the best extent. Another advantage of polystyrene is that the resulting graphene surface is free of residues from the transfer polymer. [25, 32] Ethyl acetate is known to swell PDMS slightly. [41] Hence, in order to minimize the contact between ethyl acetate and PDMS, the removal of polystyrene was carried out by flowing a minimal amount of solvent (ca. 1 mL) using a micropipette.

Although the transfer using polystyrene / ethylacetate on a mildly activated PDMS surface yielded intact large area (few cm^2) graphene, we observed, to our surprise, that the stability post transfer was quite limited. When the samples were immersed in water immediately after transfer, often the graphene sheet rolled up and partly detached from the PDMS surface. Most likely, water as a polar solvent interacts strongly with the plasma-treated PDMS surface due to the high surface energy and the hydrophilic nature. [21, 26] Hence, the water molecules are most likely able to diffuse below the graphene sheet, weakening the adhesion of the less polar graphene sheet to the PDMS surface. Interestingly, we observed that the damage to graphene was less severe, when the samples were immersed in water several days after the transfer was complete. A related aspect with PDMS (without graphene) is that the surface energy slowly

decreases over time (even under ambient conditions), as inferred from an increase in contact angle, shown by the filled squares in figure 2(a). Such a variation in the contact angle of PDMS

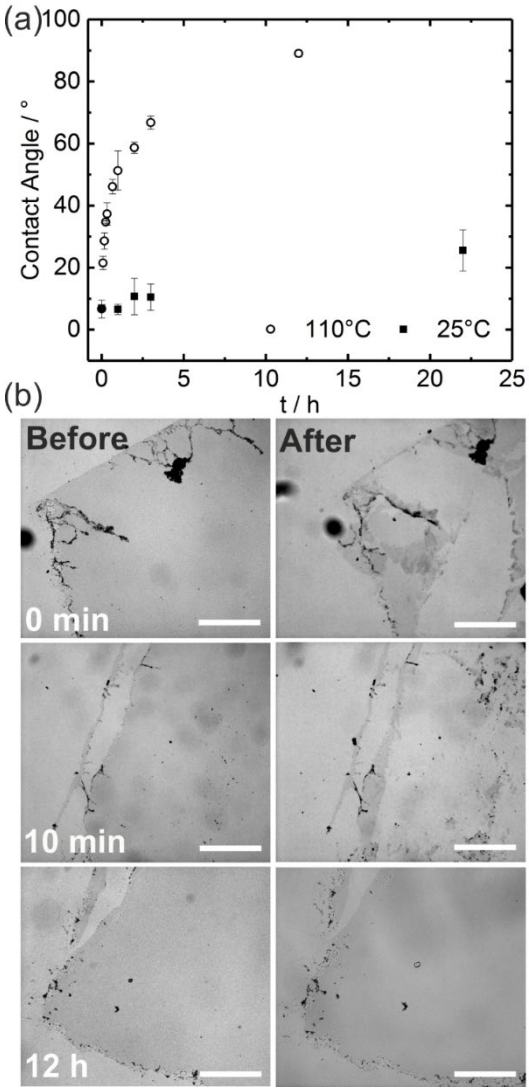

Figure 2. (a) Water contact angle measured on PDMS (without graphene) as a function of annealing time at two different temperatures. (b) Optical images of graphene sheets transferred on to PDMS substrates annealed at 110°C for the indicated times. The left column shows images before immersion in water, while the right column shows the same locations after agitation in water (10 min. in an orbital shaker). Scale bar 50 μm.

is due to a progressive loss of wettability over days, which is referred to as hydrophobic recovery as reported earlier. [54, 57-58] Often, this is attributed to several factors including the diffusion of silanol groups and the exchange of monomers with the molecules on the surface, due to which PDMS slowly regains its original surface (energy) characteristics. [52]

We decided to follow a strategy, wherein we tried to restore the original surface energy, based on the hypothesis that a non-polar surface (or equivalently a surface with high surface energy)

would weaken the interaction with the water molecules and limit the diffusion of water below graphene. [35] This should then diminish the chance of graphene peeling off from the graphene surface. We found out that annealing the PDMS samples led to a faster restoration of the high surface energy, as attested by the decrease in water contact angle shown in figure 2(a) (open circles). We recorded optical images showing the result of immersion in water (with agitation) before and after the annealing process (figure 2(b)). Indeed, by optimizing the annealing time, we found that the stability of Gr/PDMS in water could be perfectly guaranteed after annealing the Gr/PDMS stack at 110°C for 12 h.

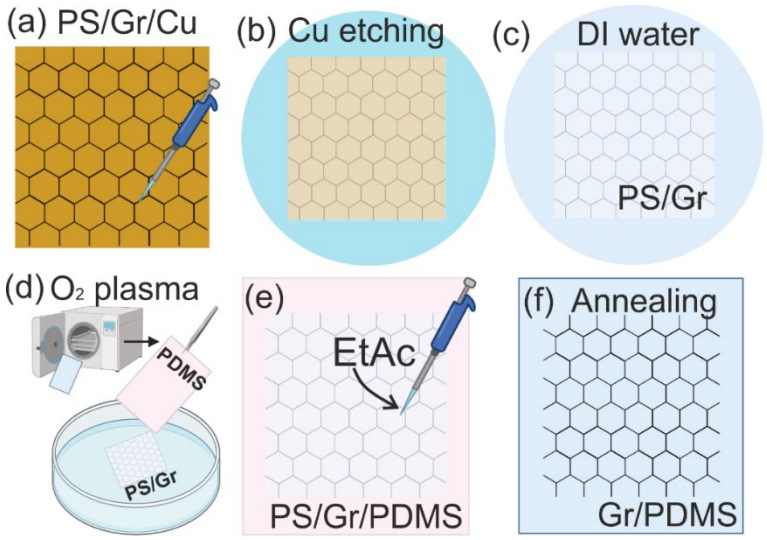

Figure 3. Scheme showing the optimized process for transferring CVD-graphene on to PDMS. (a) Graphene on a copper foil (Gr/Cu) is coated with polystyrene (PS). (b) The copper layer is etched in a solution of H_2O_2/HCl after letting the PS/Gr/Cu to swim on it. (c) By exchanging the solution in the beaker, PS/Gr is rinsed twice in water. (d) The PS/Gr slab is scooped out using a PDMS sample that is pre-treated with mild O_2 plasma. (e) The PS layer is removed by rinsing in ethyl acetate (EtAc), which is added dropwise. (f) Finally, the Gr/PDMS sample is annealed at 12 h in 110°C in air.

The entire optimized workflow based on these observations is presented in figure 3. First, graphene on copper is coated with polystyrene (PS) by drop casting a toluene solution of the polymer. Then the copper is etched in an acidified peroxide solution. Before transferring graphene, the PDMS surface is treated with an oxygen plasma. The PS/graphene stack is scooped out with the help of the plasma-treated PDMS surface. The samples are then dried under vacuum for 60 min to remove water trapped below graphene and improve adhesion.

Subsequently, PS is removed using ethyl acetate, which is added dropwise on the PS/Gr/PDMS surface. Finally, the substrate is annealed at 110°C for 12 h to complete the transfer procedure. Graphene obtained in this manner showed the characteristic *G* and *2D* vibrational modes [59] in the Raman spectrum, along with the PDMS-related modes, [60] as shown in figure 4. The defect density was found to be low as was evident from the relatively low intensity of the *D*-peak.

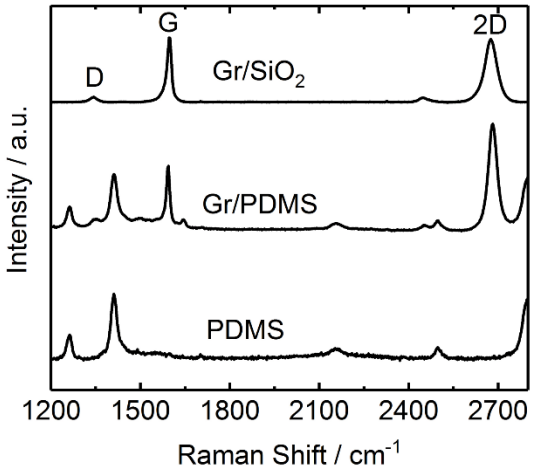

Figure 4. Raman spectrum of a bare PDMS surface, a Gr/PDMS surface and a graphene on SiO_2 surface for comparison. Laser excitation: 532 nm.

For the application of graphene as a soft electrode, it is necessary to characterize the change in stiffness of PDMS due to the presence of a single sheet of graphene. For this purpose, we transferred graphene on to a PDMS sample with prefabricated gold contacts. Figure 5(a) shows an optical image of the interface region, where the graphene sheet (in the upper half) is contacting the gold pad (on the right half). Then, we used an AFM [61-62] in Quantitative Imaging (QI) mode (Bruker / JPK) [63-64] to perform detailed nanomechanical characterization. In this mode, complete force spectra are obtained at every pixel. From these spectra, the topography and the surface stiffness can be extracted and plotted as a map as shown in figure 5(b) and 5(c) respectively. In addition, using knowledge about the scanning probe, the Young's modulus can be extracted (see figure S4 in SI for details) and plotted as a map (see figure 5(d)). From these images, it is apparent that the stiffness and the Young's modulus are both slightly higher on graphene (avg. 0.89 ± 0.10 N/m; 59 ± 14 MPa) in comparison to the bare PDMS surface (avg. 0.71 ± 0.05 N/m; 52 ± 8 MPa). (See section profiles in figure S5 in SI). The gold-covered

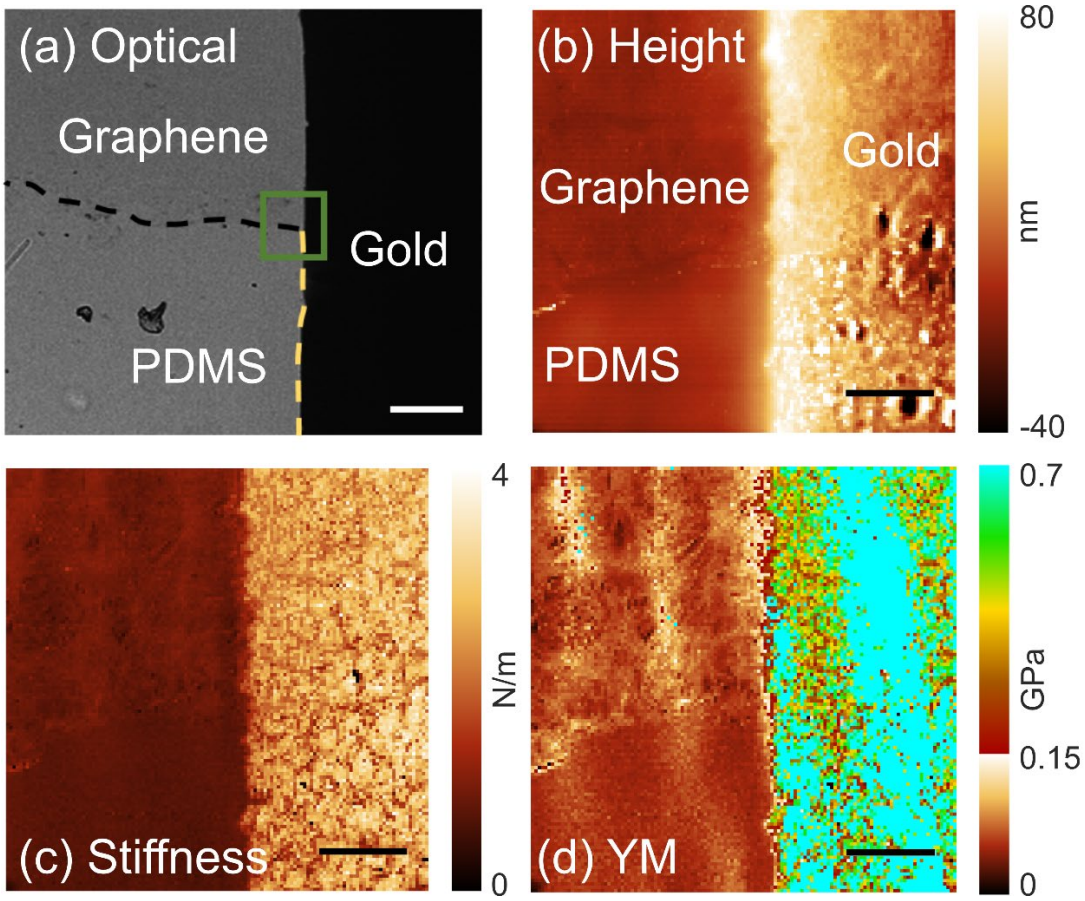

Figure 5. AFM characterization of graphene optimally transferred onto a PDMS sample with a gold contact pad. (a) Optical image showing the interface region: the right half contains a 45 nm gold film with a 5 nm chromium adhesion layer underneath; the upper left quadrant contains graphene on PDMS, while in the upper right quadrant, the graphene sheet lies on the gold film. The dashed line is a guide serving as a demarcation between the different areas. (b-d) AFM topography (Height) (b), stiffness (c) and Young's modulus – YM (d) maps of the area marked with the green rectangle in (a). See section profiles in fig. S5 in SI for further details. Scale bars: 50 µm for (a) and 2 µm for (b-d).

region, on the other hand, shows a higher average stiffness and a much higher Young's modulus (avg. 2.45 ± 0.51 N/m; 489 ± 231 MPa). Based on these observations, it is quite clear that graphene brings a clear advantage as an electrode on a soft substrate, since it affects the stiffness of the underlying PDMS to a much smaller extent (< 25%) in comparison to gold (one order of magnitude). The Young's modulus values that we extract on Au/PDMS are slightly lower than values reported in previous observations, which could be due to a difference in the preparation procedure. [12]

The values of Young's modulus in figure 5 for as-prepared PDMS are higher than typical values reported earlier. [9] We attribute the higher stiffness to the additional cross-linking that occurs

during the annealing and plasma treatment. [65] It has been proposed that the oxygen plasma treatment renders the topmost layer brittle and silica-like, [52, 66] thereby increasing the elastic modulus. [66-69] In order to mitigate this drawback, we have experimented with PDMS of differing stiffness, obtained by varying the BCA-ratio. Specifically, we could successfully obtain graphene devices on four types of PDMS prepared with BCA-ratios of 10:1, 20:1, 30:1 and 50:1. The same optimized transfer method (outlined in figure 3) could be directly used to achieve this goal. We obtained AFM-QI images immediately after PDMS preparation, after oxygen plasma and after graphene transfer (and annealing). Figure 6 presents a summary of the extracted values of Young's modulus on a typical sample of each of the four PDMS types. Consistent with previous reports [9, 61, 70] we can clearly see that the stiffness of as-prepared PDMS can be varied over an order of magnitude from 30 kPa to slightly under 1 MPa (black squares). Oxygen plasma treatment (with annealing) consistently increases the stiffness by at

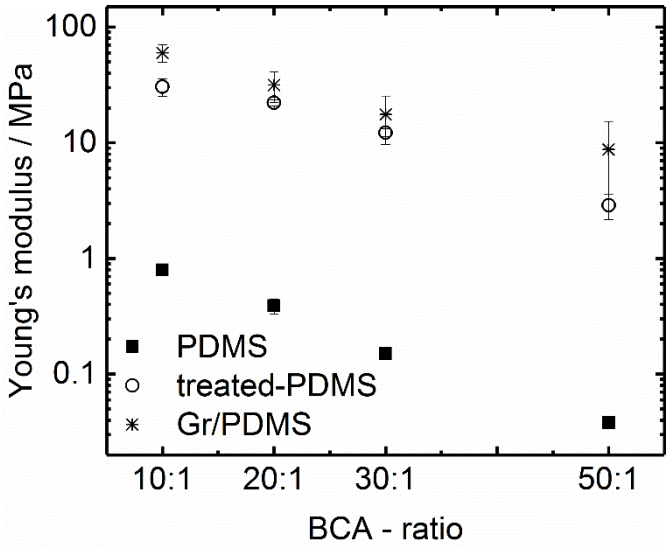

Figure 6. Evolution of Young's modulus (values extracted from AFM data) for as-prepared PDMS (filled squares) with varying BCA-ratios showing the influence of plasma treatment (open circles) and the presence of graphene (asterisks). For the two latter cases (open circles and asterisks), the samples were finally annealed at 110°C for 12 h.

least a factor of 40 (open circles), similar to previous observations. [65, 69] The presence of graphene increases this value further by at most a factor of 2 for low BCA-ratio and by a factor of 3 for a BCA-ratio of 50:1 (asterisks). Nevertheless, it is clear that, although PDMS becomes stiffer with graphene, we are able to modulate the stiffness of the graphene-transferred PDMS

surface in the range of 8 – 60 MPa. Gr/PDMS with lower values of Young's modulus was difficult to achieve. For true imitation of the ECM we will need soft electrodes with Young's modulus in the sub-MPa range. [71] In the future, we plan to explore graphene transfer on to other materials such as hydrogels to achieve Young's modulus in the sub-MPa range.

Finally, as a proof-of-principle, we have evaluated the Gr/PDMS electrodes as sensors for monitoring cell adhesion kinetics utilizing EIS. The adhesion behavior of cells to an extracellular substrate governs several cellular processes such as cell migration or the behavior of malignant cells. [1, 72] By studying the kinetics of cell adhesion to substrates, we can understand the factors affecting this process. For instance, this will help us engineer strategies for cancer therapy. Several models have been proposed for the kinetics and thermodynamics of cell adhesion. [72-74] Optical methods are typically used to monitor the process of cell adhesion. However, the time resolution is limited by the constraint to acquire images. In contrast, electrical methods have the advantage of observing the cell adhesion response in real time.

We first verified the possibility to use the fabricated electrodes in electroanalysis by measuring the redox behavior of classical redox active species such as ferrocenedimethanol and hexaminеruthenium. Both species were found to be quasi-reversible at the surface of Gr/PDMS (see figure S6 in SI for details). Moreover, based on the impedance spectra in the presence of redox species, we can model the graphene-liquid interface as a Randles circuit, with the solution resistance, the double layer capacitance and the charge transfer resistance as the key components (see figure S7 in SI).

For the cell experiments, we used a small home-built electrochemical cell, which was mounted on an inverted microscope with the capability of live-cell imaging using phase contrast. (see figure 7a, top). Miniature counter and homemade reference electrodes were used, with the contacted graphene sheet acting as the working electrode. Furthermore, the whole measurement chamber was temperature-controlled at 37 °C in a 5% CO_2 atmosphere. We simultaneously recorded phase contrast images (one image every minute during the first hour and every 5

minutes later on) during the continuous recording of impedance spectra. This helped us correlate cell (adhesion) behavior with the signals in the real-time impedance measurements. When cells adhere to the graphene surface, they constitute a barrier for the flow of electrons and thereby increase the interfacial resistance. At the same time, cells are non-conducting and constitute an additional interfacial capacitance, which occurs in series with the electrical double layer. [46-47] The change in resistance can be recorded at low frequencies, while the capacitance variations are best monitored at high frequencies (figure 7a, bottom).

Figure 7(b) shows the evolution of the impedance (black curve – resistance; blue curve – capacitance) during the attachment and spreading of MCF-7 epithelial breast cancer cells [48] on a Gr/PDMS electrode. In the absence of redox species, the interface can be modelled as a resistor and non-ideal-capacitor in series (see figure S8 in SI). A selection of simultaneously recorded phase contrast images are shown in figure 7(c). The Gr/PDMS sample was previously modified with a layer of fibronectin (FN), which is known to promote cell adhesion. [75] Initially (t = 0 h), the culture medium (see methods for details of cell culture) was placed on the FN/Gr/PDMS surface. The cells were subsequently seeded in the sample volume (at the time indicated by the red arrow). All along until t = 27 h, we can see that the resistance increases while the capacitance decreases, consistent with the continuous attachment of the cells on to the graphene surface, as also evident in the optical images.

The interaction of cells with a substrate is a highly complex process depending on several factors including cell type, cell culture conditions, etc. [49] Despite this complexity, the kinetics of the impedance change in figure 7(b) shows some features based on which, we can identify three different phases, reminiscent of a multi-step process often discussed in the literature. [72] In phase I, we see a slow increase in resistance and a saturation, which we attribute to the initial sedimentation of cells on to the sensor surface. In this phase, the cells are still round and the process of adhesion has not set in yet (optical image at 3 h). Since sedimentation increases the local concentration of cells close to the electrode, the effective dielectric constant is expected

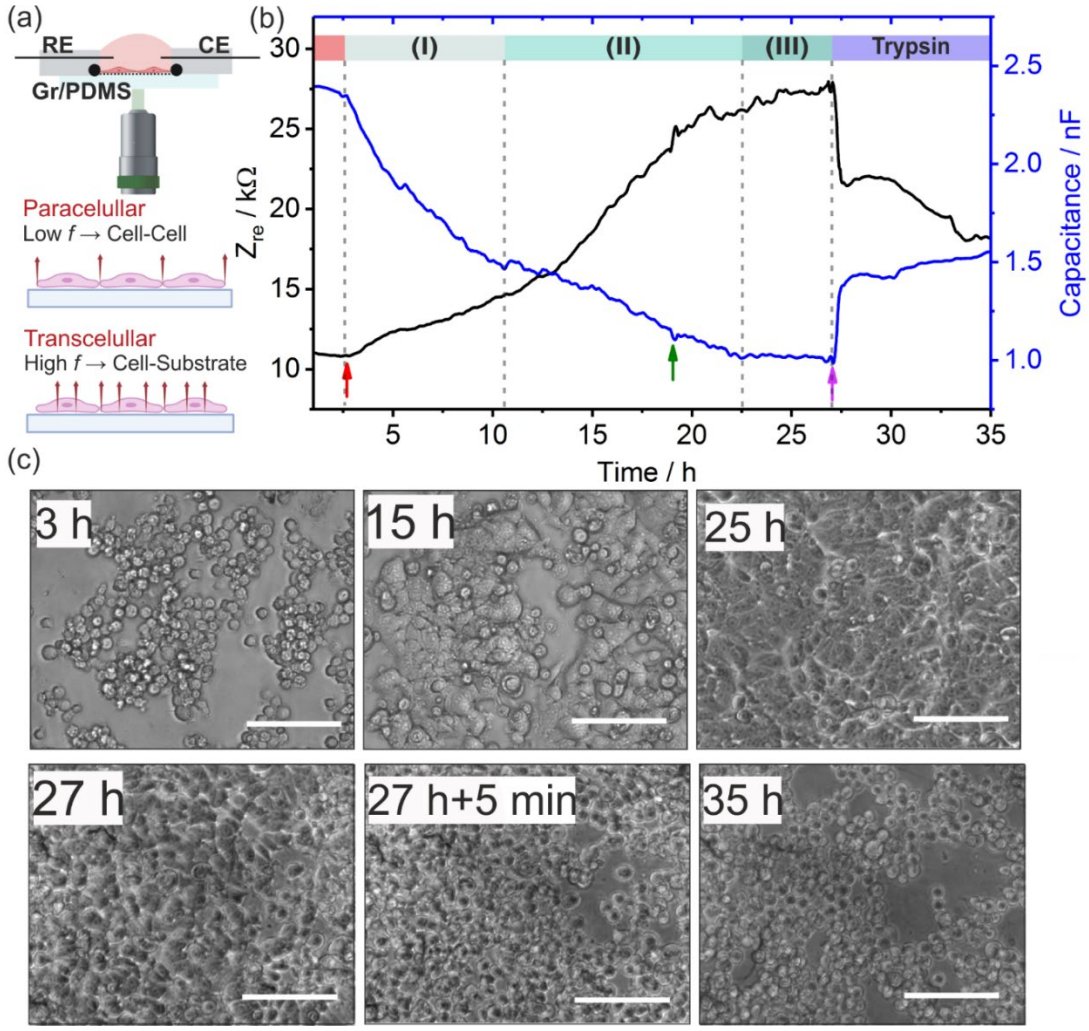

Figure 7. Real-time monitoring of the adhesion kinetics of MCF-7 cancer cells on to Gr/PDMS coated with 10 µg/mL FN. (a) (top) Scheme showing the measurement setup, where an electrochemical cell is prepared on an inverted microscope, which is equipped with the capability for live cell imaging. Gr serves as the working electrode. RE: reference electrode, CE: counter electrode. (bottom) Scheme showing the different interactions that can be detected by EIS through an appropriate choice of the detection frequency. (b) Evolution of the real part of impedance (Zre at 400 Hz) and the capacitance (extracted at 40 kHz) measured in culture medium during cell adhesion on to and detachment from graphene. Red arrow corresponds to the addition of 1.6 x 105 cells to the culture medium; green arrow corresponds to an intermediate rinsing step to refresh the culture medium; magenta arrow corresponds to the addition of 0.05% trypsin to induce the detachment of the adhered cells. I, II and III refer to three phases of adhesion – see text for details. (c) Phase contrast live images acquired simultaneously during the EIS measurement in (b). Scale bar is 100 µm.

to reduce, which results in a decrease in capacitance. In phase II, we see a faster near-exponential increase in resistance, which we attribute to the attachment of cells and subsequent flattening through integrin-based binding to the FN on graphene (as also confirmed by the optical image at t = 15 h). Specifically, for MCF-7 cells, the resistance increase is also partially due to the formation of cell-cell junctions, as has been observed earlier. [48] In this phase, the capacitance decrease is comparatively low. This can be understood by considering that the cells,

which already sediment on to the surface during phase I, undergo morphological changes during adhesion, thereby bringing relatively smaller changes in capacitance. In phase III, a confluent layer of cells is established (optical image at t = 25 h). Here, the change in impedance is of a relatively small amplitude. This is consistent with spreading of the confluent cells including a local reorganization of cellular components or cellular motion. [46, 72, 76] The green arrow indicates the point where the culture medium is replenished with simultaneous removal of non-adhered cells. Similar real-time adhesion kinetics with a multi-step behavior could be qualitatively observed on other devices. It is important to note here that the choice of the frequency is crucial to interpret the interaction kinetics of the cells with the graphene surface properly. Since we acquire the entire impedance spectrum continuously, this choice can be made after data acquisition. Glimpses of complete impedance spectra in the different phases are shown in figure S9 in SI.

In order to validate our methodology further, we used trypsin, which forces the detachment of the adhered cells from the fibronectin layer. [77] The detachment depends on the concentration and incubation time. At t = 27 h 0.05% trypsin is added to the culture media. Soon after addition, we see a reversal in the resistance / capacitance time profile. The resistance decreases while the capacitance increases signifying a detachment of the cells from the graphene surface. This correlates very well with the clear change in morphology from flattened cells (phase contrast image, t = 27 h) to rounded cells (image at t = 27 h + 5 min). The time required for detachment (~ 5 min) agrees well with previous reports for cell detachment performed at the chosen trypsin concentration. [77] After detachment, the cells diffuse away from the surface slowly, which can be seen as a slow change in impedance during the incubation with trypsin. In the optical image a corresponding reduction in concentration of cells close to the sensor surface (t = 35 h) is discernible. In principle, such a sensor would be typically for single use. Since the impedance response is qualitatively similar from one device to another, we can use a fresh Gr/PDMS sensor for every sensor trial. With this, we have clearly demonstrated that our Gr/PDMS sensors are

able to monitor complex cellular interactions with a soft and flexible underlying surface in a reliable manner.

CONCLUSION

In summary, we have demonstrated that by tuning the surface energy of the substrate before, during and after the transfer process, it is possible to obtain large area intact graphene sheets on PDMS. We believe that such an approach is generic enough and can be pursued on other substrates, in order to obtain as large an area of persistently adhered graphene as possible. We could also clearly prove that graphene – in comparison to gold – is best suited as an electrode on a soft substrate, since the underlying stiffness is only slightly affected. We were successful in deciphering cellular interactions using mm-sized graphene electrodes on the soft substrate without the need for micropatterning, which is typically required for other electrode materials. [46, 78] In the future, micropatterning can be additionally exploited to investigate variations in achievable detection sensitivity. It is known that not only the substrate stiffness but also other interfacial properties such as surface charge, hydrophilicity and bioactivity of the substrate have an effect on the interaction behavior of cells with surfaces. [79] The proposed methodology is a first step for obtaining routine electrodes on PDMS. In general, our work suggests that optimizing the surface energy during graphene transfer can serve as a generic pathway for obtaining graphene on arbitrary soft and flexible substrates. Through chemical functionalization, these physicochemical properties can be modulated, using which we can modulate cell adhesion [79-80] and thereby obtain a better picture of the exact role played by such interactions on cell adhesion.

EXPERIMENTAL SECTION

Chemicals. 1,1'-ferrocenedimethanol, polystyrene (PS, av. Mw 35000) and toluene (≥ 99.8 %, Rotisolv®) were purchased from Sigma-Aldrich; toluene and ethanol from Roth, acetone and isopropanol in VLSI quality from BASF. CVD-graphene on polished copper foil was purchased

from Graphenea. All solutions were prepared with ultra-pure water (Barnstead Easypure II system, 18.2 MΩ.cm^{-1}).

As-prepared PDMS. The PDMS is prepared by mixing the base and curing agent from a commercial SYLGARD™ 184 Silicone Elastomer Kit (DC-184, Dow Corning). Uncured solution is then poured over a flat surface (a glass wafer or a plastic petri dish), and degassed for 30 minutes. Afterwards, the PDMS is cured at 60°C for 1 h.

Graphene transfer. A polystyrene solution with a concentration of 50 mg/mL in toluene is drop-cast onto a CVD-graphene copper foil. The sample is then heated at 60°C for 15 minutes in a convection oven to form a polymer layer, which will serve as a support for the subsequent transfer process. Next, the copper foil is removed by immersing the sample in an etching solution (1:3:16 v/v H_2O_2:HCl:H_2O). This step allows the polystyrene layer, along with the graphene sheet, to be transferred to a PDMS substrate. Before transfer, the PDMS substrate is treated with oxygen plasma for 5 seconds at 50 W and 0.3 mbar to activate its surface. The activated PDMS is then used to scoop out the PS/Gr slab. Excess water is carefully removed using pressurized air. The samples are subsequently dried in a desiccator for 30 minutes and then further dried at 60°C for 1 hour. To remove the polystyrene layer, the sample surface is rinsed locally with ethyl acetate using a pipette. The sample is then dried at 75°C for 10 minutes. Finally, the Gr/PDMS sample is annealed at 110°C for 12 hours to ensure proper attachment and stability. In addition to polystyrene and toluene, poly(vinylacetate) (PVAc) as support polymer and solvents such as acetone, ethanol, dimethylsulfoxide, chloroform, and tetrahydrofuran were also evaluated.

Working electrode Gr/PDMS fabrication. Contact pads were initially fabricated on PDMS by depositing a metal layer using a shadow mask. The metallic layer used was composed of Au/Cr with thicknesses of 45 nm and 5 nm, respectively. The purpose of these contact pads is to establish electrical connection to the graphene sheet. The graphene sheet was then transferred in a way that it is in touch with the deposited metal. However, to ensure proper insulation of the metal contact from the liquid, a layer of polystyrene (PS) was manually spotted over the contact pad and dried immediately.

Surface characterization. The optical images were collected using a Leica DM4000B fluorescence microscope. A Bruker JPK Nanowizard 4 was used for AFM imaging. The details of Quantitative Imaging (QI) mode are discussed in SI. Raman spectra of graphene on the different supporting substrates were obtained on JASCO NRS-4100 Raman spectrometer equipped with a 1650 x 256 CCD detector (Andor; air/Peltier-cooled, operating temperature: -60°C), a 900 L/mm grating, a diode laser with excitation of 532 nm, and a 100X (NA 0.90) objective. The power was maintained at 5.6 mW for acquisitions on all the graphene samples. Each of the Raman spectra was recorded with an exposure time of 10 s and 3 accumulations.

Contact angle measurements. A custom-built contact angle measurement system was employed to measure the contact angles of the PDMS samples. The setup consits of a light source (ORLEGOL, VL49RGB), a *Z*-translation stage (Rotilabo®), a precision pipette (Eppendorf Research® plus) and a camera system (IDCP B.V., Dino-Lite, AM73915MZTL). To conduct a measurement, a 1µL droplet of deionised water was placed on the surface of the material of interest using the precision pipette. Subsequently, an image of the droplet was recorded. The recored images were processed with ImageJ using the contact angle plugin. To ensure accuracy and reproducibility, all measurements were repeated at least 6 times. The experiments were carried out under standard atmospheric conditions, without temperature control.

Electrochemical measurements. The electrochemical measurements were carried out in 10 mM phosphate buffer (pH 2.4 ± 0.2 and 7.2 ± 0.1) with added 0.1 M KCl as supporting electrolyte in a standard three-electrode set-up using an EmStat 4S PalmSens potentiostat or an Ivium Compactstat. A Pt wire was used as the counter electrode, an Ag/AgCl (3 M KCl) served as the reference electrode. All measurements were done under ambient conditions and in aqueous solutions. Cyclic voltammetry (CV) was performed at scan rates from 1 mV/s to 100 mV/s. Impedance spectra are fitted using self-written software based on a RQ-circuit for buffer solution and a Randles circuit for solutions with electroactive species. Q stands for constant phase element.

Cell culture. The human epithelial breast cancer cell line (MCF-7) was obtained from ATCC. These cells were cultured in RPMI supplemented with 10% fetal bovine serum (FBS), 1% sodium pyruvate, 1% alpha medium (MEM, 100 units/mL penicillin-streptomycin, and 1% non-essential amino acids (NEAA) at 37°C with 5% CO_2. All cell culture chemicals were from Bio & Sell, Germany. For the adhesion experiments, adherent cells were detached from the culture surface using trypsin-EDTA 0.05% (Sigma-Aldrich, Invitrogen, Germany) for 5 minutes at 37°C. Subsequently, the cells were seeded at a density of 2000 cells/mm^2 onto the functionalized electrode, followed by incubation at 37°C with 5% CO_2.

Electrochemical Impedance Sensing. A custom-designed measurement cell made of plexiglas was used for the experiment. The cell's measurement chamber was sealed with an O-ring, creating a contact area of 66.5 mm^2 with the substrate (working electrode). The cell had a total volume of 400 µL. The reference electrode (Ag/AgCl) and counter electrode (Pt) were introduced into the cell through two lateral perforations, and the chamber was securely sealed with dental glue to prevent any leakage. During the experiment, electrochemical impedance spectra were recorded using the potentiostat, while MCF-7 cells were attaching and spreading on Gr/PDMS electrodes. Simultaneously, time-resolved phase contrast microscopy was employed to provide a more detailed view of the cellular process. The phase contrast microscopy was performed using an inverted microscope (Nikon Eclipse Ti2) with an integrated incubator to maintain the proper conditions for promoting cell attachment (37°C, 5% CO_2). All electrochemical measurements were conducted within a custom-designed Faraday cage. This cage was engineered to fit seamlessly inside the incubator and did not interfere with the optical path of the microscope. This ensured that the electrochemical experiments were shielded from external electromagnetic interference, guaranteeing the accuracy and reliability of the collected data. Before seeding the MCF-7 cells, the system was allowed to stabilize at 37°C with 5% CO_2 for one hour. Impedance spectra were then recorded at open circuit potential (OCP) every 90 seconds, in the frequency range 10 to 10^5 Hz, using a sinusoidal AC voltage of 10 mV amplitude. The equivalent capacitance of the system was calculated from the imaginary part of the complex impedance at high frequencies (40 kHz) where the resistive part could be neglected. The electrode resistance was monitored at 400 Hz, corresponding to the real part of the impedance. Once the system reached a steady state, 160,000 cells were seeded. Subsequent impedance measurements were conducted with the cells present to observe and analyze the changes that occurred during the attachment and spreading process.

ACKNOWLEDGEMENTS

This project was funded by a joint initiative of the Deutsche Forschungsgemeinschaft (DFG, German Research Foundation) (projects: 431849238; INST 276/754-1) and CONICET (project: 23120180100103CO). Partial funding from the DFG as part of the excellence initiative *via* the Graduate School of Analytical Sciences Adlershof (GSC1013 SALSA) is acknowledged. This work has received funding from the European Union's Horizon 2020 research and innovation programme under the Marie Skłodowska-Curie grant agreement No.

872869. D.P. acknowledges financial support from the National Agency for the Promotion of Science and Technology (ANPCyT, PICT-2019-00905). V.G. acknowledges CONICET for a doctoral scholarship. D.P. is a staff researcher of CONICET. We thank Robert Jungnickel for help with initial AFM imaging and Prof. Rüdiger Tiemann for support in setting-up the live-cell-imaging microscope.

CONFLICT OF INTEREST

The authors declare no conflict of interest.

REFERENCES

1. Bissell, M. J.; LaBarge, M. A., Context, tissue plasticity, and cancer: Are tumor stem cells also regulated by the microenvironment? *Cancer Cell* **2005,** *7* (1), 17-23.
2. Engler, A. J.; Sen, S.; Sweeney, H. L.; Discher, D. E., Matrix Elasticity Directs Stem Cell Lineage Specification. *Cell* **2006,** *126* (4), 677-689.
3. Gao, D.; Parida, K.; Lee, P. S., Emerging Soft Conductors for Bioelectronic Interfaces. *Adv. Funct. Mater.* **2020,** *30* (29), 1907184.
4. He, S.; Zhang, Y.; Gao, J.; Nag, A.; Rahaman, A., Integration of Different Graphene Nanostructures with PDMS to Form Wearable Sensors. *Nanomaterials (Basel)* **2022,** *12* (6).
5. Kim, J.; Ghaffari, R.; Kim, D.-H., The quest for miniaturized soft bioelectronic devices. *Nat. Biomed. Engg.* **2017,** *1* (3), 0049.
6. Saffioti, N. A.; Cavalcanti-Adam, E. A.; Pallarola, D., Biosensors for Studies on Adhesion-Mediated Cellular Responses to Their Microenvironment. *Frontiers in Bioengineering and Biotechnology* **2020,** *8*.
7. Chitrakar, C.; Hedrick, E.; Adegoke, L.; Ecker, M., Flexible and Stretchable Bioelectronics. *Materials (Basel)* **2022,** *15* (5).
8. Sutthiwanjampa, C.; Hong, S.; Kim, W. J.; Kang, S. H.; Park, H., Hydrophilic Modification Strategies to Enhance the Surface Biocompatibility of Poly(dimethylsiloxane)-Based Biomaterials for Medical Applications. *Adv. Mater. Interf.* **2023,** *10* (12), 2202333.
9. Drebezghova, V.; Hakil, F.; Grimaud, R.; Gojzewski, H.; Vancso, G. J.; Nardin, C., Initial bacterial retention on polydimethylsiloxane of various stiffnesses: The relevance of modulus (mis)match. *Colloids Surf. B. Biointerfaces* **2022,** *217*, 112709.
10. Johnston, I. D.; McCluskey, D. K.; Tan, C. K. L.; Tracey, M. C., Mechanical characterization of bulk Sylgard 184 for microfluidics and microengineering. *J. Micromech. Microengg.* **2014,** *24* (3), 035017.
11. Seghir, R.; Arscott, S., Extended PDMS stiffness range for flexible systems. *Sens. Actuat. A* **2015,** *230*, 33-39.
12. Cortelli, G.; Patruno, L.; Cramer, T.; Murgia, M.; Fraboni, B.; de Miranda, S., Atomic Force Microscopy Nanomechanics of Hard Nanometer-Thick Films on Soft Substrates: Insights into Stretchable Conductors. *ACS Appl. Nano Mater.* **2021,** *4* (8), 8376-8382.
13. Discher, D. E.; Janmey, P.; Wang, Y.-l., Tissue Cells Feel and Respond to the Stiffness of Their Substrate. *Science* **2005,** *310* (5751), 1139-1143.
14. Yeung, T.; Georges, P. C.; Flanagan, L. A.; Marg, B.; Ortiz, M.; Funaki, M.; Zahir, N.; Ming, W.; Weaver, V.; Janmey, P. A., Effects of substrate stiffness on cell morphology, cytoskeletal structure, and adhesion. *Cell Motility* **2005,** *60* (1), 24-34.
15. Schwarz, U. S.; Safran, S. A., Physics of adherent cells. *Rev. Mod. Phys.* **2013,** *85* (3), 1327-1381.
16. Yan, L.-P.; Wen, M.-Y.; Qin, Y.; Bi, C.-X.; Zhao, Y.; Fan, W.-T.; Yan, J.; Huang, W.-H.; Liu, Y.-L., Soft Electrodes for Electrochemical and Electrophysiological Monitoring of Beating Cardiomyocytes. *Angew. Chem. Int. Ed.* **2022,** *61* (26), e202203757.

17. Tahk, D.; Lee, H. H.; Khang, D.-Y., Elastic Moduli of Organic Electronic Materials by the Buckling Method. *Macromolecules* **2009,** *42* (18), 7079-7083.
18. Du, J.; Tong, B.; Yuan, S.; Dai, N.; Liu, R.; Zhang, D.; Cheng, H.-M.; Ren, W., Advances in Flexible Optoelectronics Based on Chemical Vapor Deposition-Grown Graphene. *Adv. Funct. Mater.* **2022,** *32* (42), 2203115.
19. Kuzum, D.; Takano, H.; Shim, E.; Reed, J. C.; Juul, H.; Richardson, A. G.; de Vries, J.; Bink, H.; Dichter, M. A.; Lucas, T. H.; Coulter, D. A.; Cubukcu, E.; Litt, B., Transparent and flexible low noise graphene electrodes for simultaneous electrophysiology and neuroimaging. *Nat. Commun.* **2014,** *5* (1), 5259.
20. Chen, M.; Haddon, R. C.; Yan, R.; Bekyarova, E., Advances in transferring chemical vapour deposition graphene: a review. *Materials Horizons* **2017,** *4* (6), 1054-1063.
21. Chen, Y.; Gong, X.-L.; Gai, J.-G., Progress and Challenges in Transfer of Large-Area Graphene Films. *Advanced Science* **2016,** *3* (8), 1500343.
22. Gao, Y.; Chen, J.; Chen, G.; Fan, C.; Liu, X., Recent Progress in the Transfer of Graphene Films and Nanostructures. *Small Methods* **2021,** *5* (12), 2100771.
23. Qing, F.; Zhang, Y.; Niu, Y.; Stehle, R.; Chen, Y.; Li, X., Towards large-scale graphene transfer. *Nanoscale* **2020,** *12* (20), 10890-10911.
24. Ullah, S.; Yang, X.; Ta, H. Q.; Hasan, M.; Bachmatiuk, A.; Tokarska, K.; Trzebicka, B.; Fu, L.; Rummeli, M. H., Graphene transfer methods: A review. *Nano Research* **2021,** *14* (11), 3756-3772.
25. Langston, X.; Whitener, K. E., Graphene Transfer: A Physical Perspective. *Nanomaterials* **2021,** *11* (11), 2837.
26. Martins, L. G. P.; Song, Y.; Zeng, T.; Dresselhaus, M. S.; Kong, J.; Araujo, P. T., Direct transfer of graphene onto flexible substrates. *Proc. Natl. Acad. Sci. USA* **2013,** *110* (44), 17762-17767.
27. Kang, S. J.; Kim, B.; Kim, K. S.; Zhao, Y.; Chen, Z.; Lee, G. H.; Hone, J.; Kim, P.; Nuckolls, C., Inking Elastomeric Stamps with Micro-Patterned, Single Layer Graphene to Create High-Performance OFETs. *Adv. Mater.* **2011,** *23* (31), 3531-3535.
28. Kim, K. S.; Zhao, Y.; Jang, H.; Lee, S. Y.; Kim, J. M.; Kim, K. S.; Ahn, J.-H.; Kim, P.; Choi, J.-Y.; Hong, B. H., Large-scale pattern growth of graphene films for stretchable transparent electrodes. *Nature* **2009,** *457* (7230), 706-710.
29. Jung, W.; Kim, D.; Lee, M.; Kim, S.; Kim, J.-H.; Han, C.-S., Ultraconformal Contact Transfer of Monolayer Graphene on Metal to Various Substrates. *Adv. Mater.* **2014,** *26* (37), 6394-6400.
30. Lee, Y.; Bae, S.; Jang, H.; Jang, S.; Zhu, S.-E.; Sim, S. H.; Song, Y. I.; Hong, B. H.; Ahn, J.-H., Wafer-Scale Synthesis and Transfer of Graphene Films. *Nano Lett.* **2010,** *10* (2), 490-493.
31. Hiranyawasit, W.; Punpattanakul, K.; Pimpin, A.; Kim, H.; Jeon, S.; Srituravanich, W., A novel method for transferring graphene onto PDMS. *Appl. Surf. Sci.* **2015,** *358*, 70-74.
32. Song, J.; Kam, F.-Y.; Png, R.-Q.; Seah, W.-L.; Zhuo, J.-M.; Lim, G.-K.; Ho, P. K. H.; Chua, L.-L., A general method for transferring graphene onto soft surfaces. *Nat. Nanotechnol.* **2013,** *8* (5), 356-362.
33. Gao, X.; Zheng, L.; Luo, F.; Qian, J.; Wang, J.; Yan, M.; Wang, W.; Wu, Q.; Tang, J.; Cao, Y.; Tan, C.; Tang, J.; Zhu, M.; Wang, Y.; Li, Y.; Sun, L.; Gao, G.; Yin, J.; Lin, L.; Liu, Z.; Qin, S.; Peng, H., Integrated wafer-scale ultra-flat graphene by gradient surface energy modulation. *Nat. Commun.* **2022,** *13* (1), 5410.
34. Jang, H.; Kang, I.-S.; Lee, Y.; Cha, Y. J.; Yoon, D. K.; Ahn, C. W.; Lee, W., Direct transfer of multilayer graphene grown on a rough metal surface using PDMS adhesion engineering. *Nanotechnol.* **2016,** *27* (36), 365705.

35. Calado, V. E.; Schneider, G. F.; Theulings, A. M. M. G.; Dekker, C.; Vandersypen, L. M. K., Formation and control of wrinkles in graphene by the wedging transfer method. *Appl. Phys. Lett.* **2012,** *101* (10), 103116.
36. Xie, W.; Weng, L.-T.; Ng, K. M.; Chan, C. K.; Chan, C.-M., Clean graphene surface through high temperature annealing. *Carbon* **2015,** *94*, 740-748.
37. Wehrhold, M.; Neubert, T. J.; Yadav, A.; Vondráček, M.; Iost, R. M.; Honolka, J.; Balasubramanian, K., pH sensitivity of interfacial electron transfer at a supported graphene monolayer. *Nanoscale* **2019,** *11* (31), 14742-14756.
38. Jungnickel, R.; Mirabella, F.; Stockmann, J. M.; Radnik, J.; Balasubramanian, K., Graphene-on-gold surface plasmon resonance sensors resilient to high-temperature annealing. *Anal. Bioanal. Chem.* **2023,** *415* (3), 371-377.
39. Clarson, S. J.; Dodgson, K.; Semlyen, J. A., Studies of cyclic and linear poly(dimethylsiloxanes): 19. Glass transition temperatures and crystallization behaviour. *Polymer* **1985,** *26* (6), 930-934.
40. Hong, T.; Shen, T.; Yang, J.; Sun, Y.; Zhang, J.; Pan, H.; Hong, Y.; Wang, Y.; Chen, S.; Zhao, Y.; Guo, C. F., Sugar transfer of nanomaterials and flexible electrodes. *International Journal of Smart and Nano Materials* **2020,** *11* (1), 1-10.
41. Lee, J. N.; Park, C.; Whitesides, G. M., Solvent Compatibility of Poly(dimethylsiloxane)-Based Microfluidic Devices. *Anal. Chem.* **2003,** *75* (23), 6544-6554.
42. Roca-Cusachs, P.; Conte, V.; Trepat, X., Quantifying forces in cell biology. *Nat. Cell Biol.* **2017,** *19* (7), 742-751.
43. Stubb, A.; Laine, R. F.; Miihkinen, M.; Hamidi, H.; Guzmán, C.; Henriques, R.; Jacquemet, G.; Ivaska, J., Fluctuation-Based Super-Resolution Traction Force Microscopy. *Nano Lett.* **2020,** *20* (4), 2230-2245.
44. Pothapragada, S. P.; Gupta, P.; Mukherjee, S.; Das, T., Matrix mechanics regulates epithelial defence against cancer by tuning dynamic localization of filamin. *Nat. Commun.* **2022,** *13* (1), 218.
45. Wang, S.; Zhang, J.; Gharbi, O.; Vivier, V.; Gao, M.; Orazem, M. E., Electrochemical impedance spectroscopy. *Nature Reviews Methods Primers* **2021,** *1* (1), 41.
46. Giaever, I.; Keese, C. R., Micromotion of mammalian cells measured electrically. *Proc. Natl. Acad. Sci. USA* **1991,** *88* (17), 7896-7900.
47. Wegener, J.; Keese, C. R.; Giaever, I., Electric Cell–Substrate Impedance Sensing (ECIS) as a Noninvasive Means to Monitor the Kinetics of Cell Spreading to Artificial Surfaces. *Exp. Cell Res.* **2000,** *259* (1), 158-166.
48. Pallarola, D.; Bochen, A.; Guglielmotti, V.; Oswald, T. A.; Kessler, H.; Spatz, J. P., Highly Ordered Gold Nanopatterned Indium Tin Oxide Electrodes for Simultaneous Optical and Electrochemical Probing Cell Interactions. *Anal. Chem.* **2017,** *89* (18), 10054-10062.
49. Wegener, J.; Janshoff, A.; Galla, H. J., Cell adhesion monitoring using a quartz crystal microbalance: comparative analysis of different mammalian cell lines. *Eur. Biophys. J.* **1998,** *28* (1), 26-37.
50. Wehrhold, M.; Neubert, T. J.; Grosser, T.; Vondráček, M.; Honolka, J.; Balasubramanian, K., A highly durable graphene monolayer electrode under long-term hydrogen evolution cycling. *Chem. Commun.* **2022,** *58* (23), 3823-3826.
51. Zhou, J.; Khodakov, D. A.; Ellis, A. V.; Voelcker, N. H., Surface modification for PDMS-based microfluidic devices. *Electrophoresis* **2012,** *33* (1), 89-104.
52. Owen, M. J.; Smith, P. J., Plasma treatment of polydimethylsiloxane. *J. Adhes. Sci. Technol.* **1994,** *8* (10), 1063-1075.
53. Kim, H. H.; Lee, S. K.; Lee, S. G.; Lee, E.; Cho, K., Wetting-Assisted Crack- and Wrinkle-Free Transfer of Wafer-Scale Graphene onto Arbitrary Substrates over a Wide Range of Surface Energies. *Adv. Funct. Mater.* **2016,** *26* (13), 2070-2077.

54. Bodas, D.; Khan-Malek, C., Hydrophilization and hydrophobic recovery of PDMS by oxygen plasma and chemical treatment—An SEM investigation. *Sens. Actuat. B* **2007,** *123* (1), 368-373.
55. Hegemann, D.; Gaiser, S., Plasma surface engineering for manmade soft materials: a review. *J. Phys. D: Appl. Phys.* **2022,** *55* (17), 173002.
56. Du, F.; Duan, H. L.; Xiong, C. Y.; Wang, J. X., Substrate wettability requirement for the direct transfer of graphene. *Appl. Phys. Lett.* **2015,** *107* (14), 143109.
57. Fritz, J. L.; Owen, M. J., Hydrophobic Recovery of Plasma-Treated Polydimethylsiloxane. *The Journal of Adhesion* **1995,** *54* (1-4), 33-45.
58. Hillborg, H.; Tomczak, N.; Olàh, A.; Schönherr, H.; Vancso, G. J., Nanoscale Hydrophobic Recovery: A Chemical Force Microscopy Study of UV/Ozone-Treated Cross-Linked Poly(dimethylsiloxane). *Langmuir* **2004,** *20* (3), 785-794.
59. Ferrari, A. C.; Basko, D. M., Raman spectroscopy as a versatile tool for studying the properties of graphene. *Nat. Nanotechnol.* **2013,** *8* (4), 235-246.
60. Esteves, A. C. C.; Brokken-Zijp, J.; Laven, J.; Huinink, H. P.; Reuvers, N. J. W.; Van, M. P.; de With, G., Influence of cross-linker concentration on the cross-linking of PDMS and the network structures formed. *Polymer* **2009,** *50* (16), 3955-3966.
61. Raczkowska, J.; Prauzner-Bechcicki, S.; Lukes, J.; Sepitka, J.; Bernasik, A.; Awsiuk, K.; Paluszkiewicz, C.; Pabijan, J.; Lekka, M.; Budkowski, A., Physico-chemical properties of PDMS surfaces suitable as substrates for cell cultures. *Appl. Surf. Sci.* **2016,** *389*, 247-254.
62. Liu, B.; Fu, J., Modulating surface stiffness of polydimethylsiloxane (PDMS) with kiloelectronvolt ion patterning. *J. Micromech. Microengg.* **2015,** *25* (6), 065006.
63. Bhat, S. V.; Sultana, T.; Körnig, A.; McGrath, S.; Shahina, Z.; Dahms, T. E. S., Correlative atomic force microscopy quantitative imaging-laser scanning confocal microscopy quantifies the impact of stressors on live cells in real-time. *Sci. Rep.* **2018,** *8* (1), 8305.
64. Chopinet, L.; Formosa, C.; Rols, M. P.; Duval, R. E.; Dague, E., Imaging living cells surface and quantifying its properties at high resolution using AFM in QI™ mode. *Micron* **2013,** *48*, 26-33.
65. Yang, Y.; Kulangara, K.; Lam, R. T. S.; Dharmawan, R.; Leong, K. W., Effects of Topographical and Mechanical Property Alterations Induced by Oxygen Plasma Modification on Stem Cell Behavior. *ACS Nano* **2012,** *6* (10), 8591-8598.
66. Béfahy, S.; Lipnik, P.; Pardoen, T.; Nascimento, C.; Patris, B.; Bertrand, P.; Yunus, S., Thickness and Elastic Modulus of Plasma Treated PDMS Silica-like Surface Layer. *Langmuir* **2010,** *26* (5), 3372-3375.
67. Bar, G.; Delineau, L.; Häfele, A.; Whangbo, M. H., Investigation of the stiffness change in, the indentation force and the hydrophobic recovery of plasma-oxidized polydimethylsiloxane surfaces by tapping mode atomic force microscopy. *Polymer* **2001,** *42* (8), 3627-3632.
68. Mills, K. L.; Zhu, X.; Takayama, S.; Thouless, M. D., The mechanical properties of a surface-modified layer on polydimethylsiloxane. *J. Mater. Res.* **2008,** *23* (1), 37-48.
69. Bartalena, G.; Loosli, Y.; Zambelli, T.; Snedeker, J. G., Biomaterial surface modifications can dominate cell–substrate mechanics: the impact of PDMS plasma treatment on a quantitative assay of cell stiffness. *Soft Matter* **2012,** *8* (3), 673-681.
70. Wala, J.; Maji, D.; Das, S., Influence of physico-mechanical properties of elastomeric material for different cell growth. *Biomed. Mater.* **2017,** *12* (6), 065002.
71. Padhi, A.; Nain, A. S., ECM in Differentiation: A Review of Matrix Structure, Composition and Mechanical Properties. *Ann. Biomed. Eng.* **2020,** *48* (3), 1071-1089.
72. Grinnell, F., Cellular Adhesiveness and Extracellular Substrata. In *Int. Rev. Cytol.*, Bourne, G. H.; Danielli, J. F., Eds. Academic Press: 1978; Vol. 53, pp 65-144.
73. Vogler, E. A., Thermodynamics of short-term cell adhesion in vitro. *Biophys. J.* **1988,** *53* (5), 759-769.

74. Škvarla, J., A physico-chemical model of microbial adhesion. *J. Chem. Soc., Faraday Trans.* **1993,** *89* (15), 2913-2921.
75. Ruoslahti, E., Fibronectin in cell adhesion and invasion. *Cancer Metastasis Rev.* **1984,** *3* (1), 43-51.
76. Giaever, I.; Keese, C. R., A morphological biosensor for mammalian cells. *Nature* **1993,** *366* (6455), 591-592.
77. Brown, M. A.; Wallace, C. S.; Anamelechi, C. C.; Clermont, E.; Reichert, W. M.; Truskey, G. A., The use of mild trypsinization conditions in the detachment of endothelial cells to promote subsequent endothelialization on synthetic surfaces. *Biomaterials* **2007,** *28* (27), 3928-3935.
78. Janshoff, A.; Kunze, A.; Michaelis, S.; Heitmann, V.; Reiss, B.; Wegener, J., Cell Adhesion Monitoring Using Substrate-Integrated Sensors. *J. Adhes. Sci. Technol.* **2010,** *24* (13-14), 2079-2104.
79. Cai, S.; Wu, C.; Yang, W.; Liang, W.; Yu, H.; Liu, L., Recent advance in surface modification for regulating cell adhesion and behaviors. *Nanotechnol. Rev.* **2020,** *9* (1), 971-989.
80. Xiao, Y.; Truskey, G. A., Effect of receptor-ligand affinity on the strength of endothelial cell adhesion. *Biophys. J.* **1996,** *71* (5), 2869-2884.